The Stabilized Biconjugate Gradient Fast Fourier Transform Method for Electromagnetic Scattering

Xue Min Xu, Qing Huo Liu and Zhong Qing Zhang

Duke University
Department of Electrical and Computer Engineering
Box 90291
Durham, NC 27708
E-mail qhliu@ee.duke.edu

Abstract–**An iterative method, the stabilized biconjugate gradient (BiCGSTAB) method, combined with the fast Fourier transform (FFT) for solving electromagnetic scattering problems is developed for the 3-D volume electric field integral equation. It converges significantly faster than the conventional conjugate gradient (CG) and biconjugate gradient (BiCG) fast Fourier transform methods. With this BCGS-FFT method, we can solve a large-scale volume integral equation with 20 million unknowns on a single CPU workstation.**

I. Introduction

In this work, we aim to develop an efficient method to solve the three-dimensional volume electric field integral equation for electromagnetic scattering problems. Our approach is based on the stabilized biconjugate-gradient fast Fourier transform (BCGS-FFT) method.

The volume integral equation formulation [1], [2] for electromagnetic scattering problems often results in discrete non-Hermitian matrix or operator equation. The conjugate gradient (CG) method used to solve the non-Hermitian discrete equation is the so-called "conjugate gradient method applied to normal equations" [3], [4]. In this paper, the CG refers to this particular version. This CG method squares the condition number of the linear system, thus has a slower convergence rate compare to a Hermitian system [5], [6]. One choice to improve the convergence speed is to use any of the following Lanczos-type [7], [8] product methods such as the biconjugate-gradient (BiCG), conjugate-gradient squared (CGS), stabilized biconjugate-gradient (BiCGSTAB), and the transpose-free quasi-minimum residual (TFQMR) methods [6],[9]-[12]. These methods solve the original equation directly, thus yielding faster convergence rate than the CG method.

A well-known problem of the Lanczos-type product methods is the danger of breakdown. This problem has been addressed in [13]-[15]. Since no breakdown has been observed in our application, we will not elaborate on this issue. Our main concern for the iterative methods is how fast it converges and how it converges is secondary.

To solve the electric field integral equation (EFIE) for electromagnetic scattering from inhomogeneous objects, the iterative solvers discussed above combined with the fast Fourier transform (FFT) are chosen. Early work in this area includes the conjugate gradient fast Fourier transform (CG-FFT) method and biconjugate gradient fast Fourier transform (BCG-FFT) method in [1], [2], [16], [17]. The iterative methods combined with FFT reduce the computational cost of solving the volume integral equation for electromagnetic scattering problem from $O(N_t^3)$ in the method of moment (MoM) to $O(KN_t \log N_t)$, where K is the number of iterations and N_t is the number of unknowns. Therefore, they are capable of solving problems with a large number of unknowns. It has been shown that two different BCG-FFT methods are more efficient than the CG-FFT method for several examples from electromagnetic scattering [2], [17]. Generally speaking, the CG-FFT method converges monotonically because it minimizes the residual at each step. On the contrary, the residual of the BCG-FFT method oscillates as it does not minimize the residual. The potential flaw of stagnation in the BiCG algorithm is addressed in [18]. Another iterative technique, the stabilized BiCG (here referred to as BiCGSTAB) method is presented in [10] for matrix equation, which converges more smoothly than the BiCG method.

In this work, we apply the iterative BiCGSTAB scheme to solve the volume electric field integral equation (EFIE) for electromagnetic scattering problems. The transpose free quasi-minimum residual (TFQMR) iterative procedure is also implemented. TFQMR is chosen for its simplicity and low computation cost compared to other QMR schemes. Numerical examples show that the BCGS-FFT method is more efficient than the CG-FFT, BCG-FFT and TFQMR-FFT methods for our applications and is capable of solving large prob-

lems.

II. Formulation

We consider the scattering problem by a lossy, inhomogeneous dielectric object with complex permittivity

$$\epsilon(\mathbf{r}) = \epsilon_0\epsilon_r(\mathbf{r}) - \frac{j\sigma(\mathbf{r})}{\omega} \tag{1}$$

where $\epsilon_r(\mathbf{r})$ is the dielectric constant inside the object, $\sigma(\mathbf{r})$ is the electric conductivity inside the object, ϵ_0 is the permittivity of free space, and ω is the angular frequency. The vectorial position in the three-dimensional space is denoted by $\mathbf{r} = x\hat{\mathbf{x}} + y\hat{\mathbf{y}} + z\hat{\mathbf{z}}$, where $\hat{\mathbf{x}}$, $\hat{\mathbf{y}}$ and $\hat{\mathbf{z}}$ are unit vectors along x, y and z direction, respectively. When the incident electric field $\mathbf{E}^i(\mathbf{r}) = (E^i_x, E^i_y, E^i_z)$ impinges on the scattering object, the volume integral equation in terms of the unknown electric flux density $\mathbf{D} = (D_x, D_y, D_z)$ over the domain V can be formulated as

$$\mathbf{E}^i(\mathbf{r}) = \frac{\mathbf{D}(\mathbf{r})}{\epsilon(\mathbf{r})} - (k_0^2 + \nabla\nabla\cdot)\mathbf{A}(\mathbf{r}), \quad \mathbf{r} \in V \tag{2}$$

where $k_0 = \omega\sqrt{\epsilon_0\mu_0}$ and the vector potential $\mathbf{A} = (A_x, A_y, A_z)$ is defined as

$$\mathbf{A}(\mathbf{r}) = \frac{1}{\epsilon_0}\int_{\mathbf{r}'\in V} g(\mathbf{r}-\mathbf{r}')\chi(\mathbf{r}')\mathbf{D}(\mathbf{r}')d\mathbf{r}' \tag{3}$$

in which the contrast function $\chi(\mathbf{r}) = \frac{\epsilon(\mathbf{r})-\epsilon_0}{\epsilon(\mathbf{r})}$, and the three-dimensional scalar Green's function is given by

$$g(\mathbf{r}) = \frac{e^{-jk_0|\mathbf{r}|}}{4\pi|\mathbf{r}|} \tag{4}$$

The weak-form discretization process follows that in [1], [17]. Both the basis and testing functions are three-dimensional rooftop functions, which are piecewise linear in the direction of the electric flux density component (D_x, D_y, D_z) and piecewise constant in the other two dimensions. We use a uniform mesh with grid widths of Δx, Δy and Δz in the x, y and z directions, respectively. The scattering object is completely embedded in the rectangular block with dimension $M\Delta x \times N\Delta y \times P\Delta z$ and the volumetric subdomain indices m, n, p satisfy $m \in [1, M]$, $n \in [1, N]$, $p \in [1, P]$. The coordinate of the center point of each volumetric subdomain is given by

$$\mathbf{r}_{m,n,p} = \{(m-0.5)\Delta x, (n-0.5)\Delta y, (p-0.5)\Delta z\} \tag{5}$$

The discrete contrast constant $\chi_{m,n,p}$ and permittivity $\epsilon_{m,n,p}$ for each cell are defined as their values at the center point $\mathbf{r}_{m,n,p}$. After discretization, the continuous equation (2) becomes

$$\begin{aligned} e^{i,(\eta)}_{m,n,p} = &\sum_{i=1}^{3}[\mathbf{b}^{(\eta)}_i \mathbf{d}^{(\eta)}_{m+(i-2)\delta_{\eta x}, n+(i-2)\delta_{\eta y}, p+(i-2)\delta_{\eta z}} \\ &+\mathbf{c}^{(\eta)}_i \mathbf{A}^{(\eta)}_{m+(i-2)\delta_{\eta x}, n+(i-2)\delta_{\eta y}, p+(i-2)\delta_{\eta z}}] \\ &+\sum_{i=1}^{2}\sum_{j=1}^{2}\mathbf{t}^{(\eta+2)}_{i,j}\mathbf{A}^{(\eta+1)}_{m_1,n_1,p_1} \\ &+\sum_{i=1}^{2}\sum_{\ell=1}^{2}\mathbf{t}^{(\eta+1)}_{i,\ell}\mathbf{A}^{(\eta+2)}_{m_2,n_2,p_2} \end{aligned} \tag{6}$$

where $\eta = x, y, z$; the subscripts are

$$\begin{aligned} m_1 &= m + (i-2)\delta_{\eta x} + (j-1)\delta_{(\eta+1)x} \\ n_1 &= n + (i-2)\delta_{\eta y} + (j-1)\delta_{(\eta+1)y} \\ p_1 &= p + (i-2)\delta_{\eta z} + (j-1)\delta_{(\eta+1)z} \\ m_2 &= m + (i-2)\delta_{\eta x} + (\ell-1)\delta_{(\eta+2)x} \\ n_2 &= n + (i-2)\delta_{\eta y} + (\ell-1)\delta_{(\eta+2)y} \\ p_2 &= p + (i-2)\delta_{\eta z} + (\ell-1)\delta_{(\eta+2)z} \end{aligned}$$

and the superscript and subscript $(\eta + i)$ follows the right hand cyclic rule, which is $x + 1 = y$, $x + 2 = z$, $y + 1 = z$, $y + 2 = x$, $z + 1 = x$ and $z + 2 = y$; and the Kronecker delta function $\delta_{\eta q} = 1$ when the $q = \eta$, and $\delta_{\eta q} = 0$ otherwise. The coefficient vector $\mathbf{b}^{(\eta)}$ and $\mathbf{c}^{(\eta)}$ are

$$\mathbf{b}^{(\eta)} = \frac{\Delta x\Delta y\Delta z\epsilon_0}{6}\begin{pmatrix} \epsilon^{-1}_{m-\delta_{\eta x}, n-\delta_{\eta y}, p-\delta_{\eta z}} \\ 2(\epsilon^{-1}_{m-\delta_{\eta x}, n-\delta_{\eta y}, p-\delta_{\eta z}} + \epsilon^{-1}_{m,n,p}) \\ \epsilon^{-1}_{m,n,p} \end{pmatrix}$$

$$\mathbf{c}^{(\eta)} = \Delta x\Delta y\Delta z\left[-\frac{k_0^2}{6}\begin{pmatrix}1\\4\\1\end{pmatrix} + (\Delta\eta)^{-2}\begin{pmatrix}-1\\2\\-1\end{pmatrix}\right]$$

and the coefficients of the matrix $\mathbf{t}^{(\eta)}$ are

$$\mathbf{t}^{(\eta)} = \Delta\eta\begin{pmatrix}-1 & 1\\ 1 & -1\end{pmatrix}$$

The values of $e^{i,(\eta)}_{m,n,p}$ are related to the incident field $E^{i,(\eta)}_{m,n,p}$ as

$$\begin{aligned} e^{i,(\eta)}_{m,n,p} = \frac{\Delta x\Delta y\Delta z}{6}[&E^{i,(\eta)}_{m+\delta_{\eta x}, n+\delta_{\eta y}, p+\delta_{\eta z}} + 4E^{i,(\eta)}_{m,n,p} \\ &+E^{i,(\eta)}_{m-\delta_{\eta x}, n-\delta_{\eta y}, p-\delta_{\eta z}}] \end{aligned} \tag{7}$$

The quantities $d^{(\eta)}_{m,n,p}$, $A^{(\eta)}_{m,n,p}$ and $E^{i,(\eta)}_{m,n,p}$ are represented by

$$d^{(\eta)}_{m,n,p} = \frac{D_\eta(\mathbf{r}_{m,n,p} - 0.5\Delta\eta\hat{\eta})}{\epsilon_0} \tag{8}$$

$$A^{(\eta)}_{m,n,p} = A_\eta(\mathbf{r}_{m,n,p} - 0.5\Delta\eta\hat{\eta}) \tag{9}$$

$$E^{i,(\eta)}_{m,n,p} = E^i_\eta(\mathbf{r}_{m,n,p} - 0.5\Delta\eta\hat{\eta}) \tag{10}$$

where $\hat{\eta}$ is the unit vector for x, y or z direction, and the vector potential can be written as a discrete convolution

$$A^{(\eta)}_{m,n,p} = \Delta x\Delta y\Delta z \cdot \sum_{m',n',p'} G_{m-m',n-n',p-p'}\chi^{(\eta)}_{m',n',p'}d^{(\eta)}_{m',n',p'}, \tag{11}$$

in which $\chi^{(\eta)}_{m,n,p}$ is the averaged value of two adjacent cells along η direction and is given by

$$\chi^{(\eta)}_{m,n,p} = \frac{\chi_{m-\delta_{\eta x}, n-\delta_{\eta y}, p-\delta_{\eta z}} + \chi_{m,n,p}}{2} \tag{12}$$

Using the convolution theorem, equation (11) can be rewritten as

$$A^{(\eta)}_{m,n,p} = \Delta x\Delta y\Delta z\mathcal{F}^{-1}\{\mathcal{F}\{[G]_{m,n,p}\}\mathcal{F}\{\chi^{(\eta)}_{m,n,p}d^{(\eta)}_{m,n,p}\}\} \tag{13}$$

where $\mathcal{F}$ and $\mathcal{F}^{-1}$ stand for discrete forward and inverse Fourier transforms, $[G]$ is the spherical mean [1] of the Green's function over the subdomain centered at $(m\Delta x, n\Delta y, p\Delta z)$ with a radius r, which satisfies

$r < \min[\Delta x, \Delta y, \Delta z]$. Equation (6) can be compactly written as a linear operator equation,

$$\mathcal{L}\mathbf{D} = \mathbf{E}^i \tag{14}$$

This equation can be solved efficiently by iterative methods for linear systems combined with the FFT algorithm for the discrete convolution in equation (13). The corresponding iterative schemes can be found in [3] for the CG method and in [6] for the BiCG method.

In this work we apply the "stabilized" BiCG (or BiCGSTAB) method [10]. It starts with an initial guess $\mathbf{D}_0$ and computes:

$$\mathbf{r}_0 = \mathbf{b} - \mathcal{L}\mathbf{D}_0 \tag{15}$$

$$\rho_0 = \alpha = \omega_0 = 1 \tag{16}$$

$$\mathbf{v}_0 = \mathbf{p}_0 = 0 \tag{17}$$

With the choice of an arbitrary vector $\hat{\mathbf{r}}_0$ such that $(\hat{\mathbf{r}}_0, \mathbf{r}_0) \neq \mathbf{0}$, e.g., $\hat{\mathbf{r}}_0 = \mathbf{r}_0$, it proceeds with

$$\rho_i = (\hat{\mathbf{r}}_0, \mathbf{r}_{i-1}); \quad \beta = (\rho_i/\rho_{i-1})(\alpha/\omega_{i-1}); \tag{18}$$

$$\mathbf{p}_i = \mathbf{r}_{i-1} + \beta(\mathbf{p}_{i-1} - \omega_{i-1}\mathbf{v}_{i-1}); \tag{19}$$

$$\mathbf{v}_i = \mathcal{L}\mathbf{p}_i; \tag{20}$$

$$\alpha = \rho_i/(\hat{\mathbf{r}}_0, \mathbf{v}_i); \tag{21}$$

$$\mathbf{s} = \mathbf{r}_{i-1} - \alpha\mathbf{v}_i; \tag{22}$$

$$\mathbf{t} = \mathcal{L}\mathbf{s}; \tag{23}$$

$$\omega_i = (\mathbf{t}, \mathbf{s})/(\mathbf{t}, \mathbf{t}); \tag{24}$$

$$\mathbf{D}_i = \mathbf{D}_{i-1} + \alpha\mathbf{p}_i + \omega_i\mathbf{s}; \tag{25}$$

$$\mathbf{r}_i = \mathbf{s} - \omega_i\mathbf{t}. \tag{26}$$

This process stops when $\mathbf{r}_i$ is small enough. One can also terminate the iteration when $||\mathbf{s}||$ is small enough. Note that the most expensive computational costs are associated with the two operations $\mathcal{L}\mathbf{p}_i$ and $\mathcal{L}\mathbf{s}$, in which an FFT algorithm is used to complete the discrete convolution kernel in equation (13). For brevity, we refer to this spectral-domain method as the BCGS-FFT method.

The BiCGSTAB iterative scheme was derived from the conjugate-gradient-squared (CGS) and BiCG methods [10]. It generates the residuals in a rather stable and more efficient way to avoid the local peaks in the convergence curve for the CGS and BiCG methods. Those local peaks may be so large that the corresponding local corrections to the current iteration result in cancelation; as a result, the final solution may have little significance in the CGS and BiCG methods. On the contrary, the residual for the nth iteration of the BiCGSTAB method can be expressed as

$$\mathbf{r}_n = Q_n(\mathcal{L})P_n(\mathcal{L})\mathbf{r}_0 \tag{27}$$

where Q_n and P_n are nth degree polynomials, $\mathcal{L}$ is a linear operator, and $\mathbf{r}_0$ is the residual of the first iteration. Note that $Q_n = 1$ and $Q_n = P_n$ for the BiCG and CGS methods, respectively, and the iterative schemes for these two methods do not minimize the residual for each iteration. In the BiCGSTAB method, this polynomial is chosen as

$$Q_n(x) = (1 - \omega_1 x)(1 - \omega_2 x) \cdots (1 - \omega_n x), \tag{28}$$

where ω_n is computed so that $\mathbf{r}_n = Q_n(\mathcal{L})P_n(\mathcal{L})\mathbf{r}_0$ is minimized in L_2-norm as a function of ω_i, which explicitly minimizes the residual for each iteration. Therefore, the BiCGSTAB method converges in a smoother and faster way. Our numerical results verify these convergence characteristics.

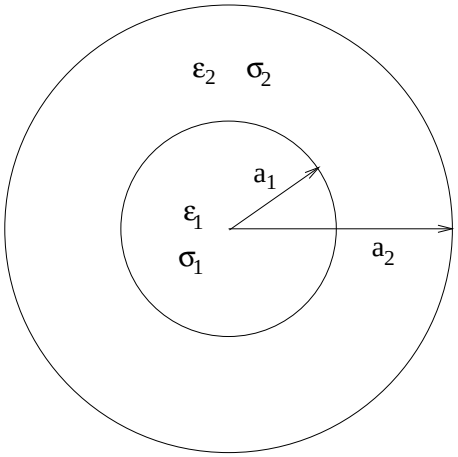

Fig. 1. Cross section of a two-layer sphere with radius a_1, permittivity ϵ_1 and conductivity σ_1 for the inner sphere, and radius a_2, permittivity ϵ_2 and conductivity σ_2 for the outer spheric coating.

III. Numerical Results

In all of the following simulations, the incident field is a plane wave with a wavelength $\lambda = 1/f\sqrt{\mu_0\epsilon_0}$ in the free space. The computational domain is a cube centered at $(0, 0, 0)$. The L_2 norm of the residual of the ith iteration is defined as

$$r_i = \frac{||\mathbf{r}_i||_2}{||\mathbf{r}_0||_2}, \quad \mathbf{r}_i = \mathcal{L}\mathbf{D}_i - \mathbf{E}^i. \tag{29}$$

Figure 1 shows the cross section of a two-layer sphere model. Figure 2 (a) and (b) shows the convergence speed of three different iterative solvers: the BiCG, BiCGSTAB and TFQMR for the two-layer sphere model presented in [1], [17] with the number of unknowns $3 \times 32 \times 31 \times 31 = 92,256$. The L_2 norm of the relative residual in Figure 2 (a) is 10^{-3} and that for Figure 2 (b) is 10^{-5}. This illustrates that the iterative solvers can converge to lower level error criteria. Note that the convergence rate of TFQMR is approximately the same as that of BiCG, as observed in [13]. However, TFQMR converges in a much smoother way than BiCG. It takes about 360 iterations for the CG method to converge to an error criteria of 10^{-3}. This convergence curve is not included for a clear view of the convergence behaviors of BiCG, BiCGSTAB and TFQMR.

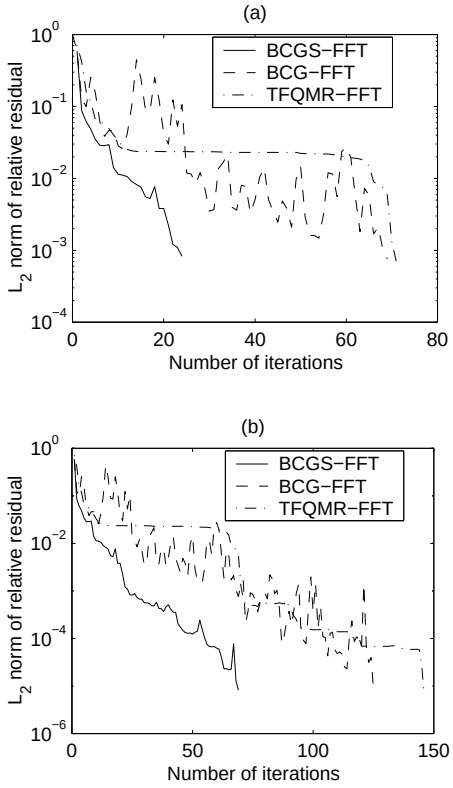

Fig. 2. Convergence curves of a two-layer sphere with $a_1 = 0.075$ m, $\epsilon_{r,1} = 72$, $\sigma_1 = 0.9$ S/m, $a_2 = 0.15$ m, $\epsilon_{r,2} = 7.5$ and $\sigma_2 = 0.05$ S/m. Error criterion is (a) 10^{-3}, and (b) 10^{-5}.

Table I compares the memory cost and CPU time of the iterative solvers. The unit of RAM is M-bytes and the unit for CPU time is second. Note that the BiCGSTAB method consumes least amount of memory and CPU time to reach the same error criteria as other iterative solvers. Therefore, the BiCGSTAB method is more suitable for our application in terms of CPU time and memory cost.

TABLE I
COMPARISON OF ITERATIVE SOLVERS

Solver	RAM	CPU	Iter. No.	CPU/iter.
BCGS	67	98	24	4.25
TFQMR	75	252	72	3.55
BiCG	96	295	69	4.33
CG	92	2030	356	5.71

Then we examine a small model of a two-layer lossy dielectric sphere, where $a_1 = 0.5$ m, $\epsilon_{r,1} = 9$, $\sigma_1 = 0.5$ S/m, $a_2 = 1.0$ m, $\epsilon_{r,2} = 4$ and $\sigma_2 = 0.2$ S/m. The frequency of the incident plane wave is 100 MHz. The magnitudes of the electric field inside the inhomogeneous two-layer sphere along the x and y axes are

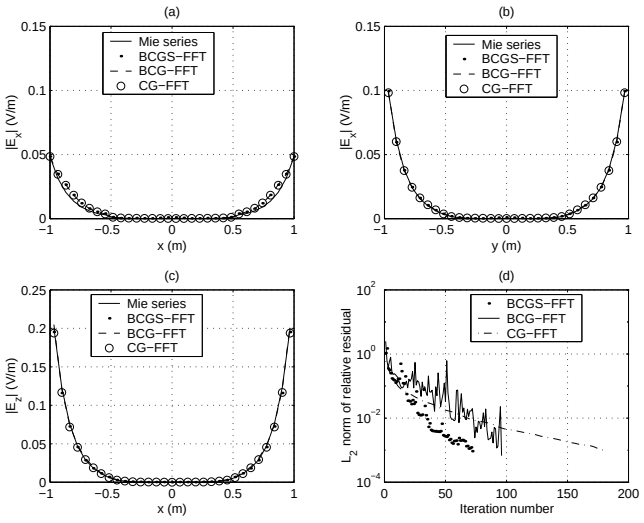

Fig. 3. (a)-(c)Electric field inside a two-layer sphere with $a_1 = 0.5$ m, $\epsilon_{r,1} = 9$, $\sigma_1 = 0.5$ S/m, $a_2 = 1.0$ m, $\epsilon_{r,2} = 4$ and $\sigma_2 = 0.2$ S/m. (d) The convergence curves.

shown in Figure 3 (a)-(c). The number of unknowns is $3 \times N_x \times N_y \times N_z = 3 \times 32 \times 31 \times 31 = 92,256$ (the factor 3 accounts for the three electric field components). Note that the BCGS-FFT, BCG-FFT and CG-FFT methods have a comparable accuracy compared with the solution from the Mie series [19]. Figure 3 (d) displays the convergence curves of those three methods. It took 175, 96 and 69 iterations for the CG-, BCG- and BCGS-FFT methods to converge to an error criteria of 0.1%, respectively. The BCGS-FFT method converges faster than the BCG-FFT method while about 2.6 times as fast as the CG-FFT method for this model. The total run time is 1147, 611 and 436 seconds for the CG-, BCG- and BCGS-FFT methods on a Sun Ultra 60 workstation (f77 compiler), respectively. Note that the difference in the computational time per iteration between the BCG- and BCGS-FFT methods is about 0.04 seconds because the BCGS-FFT method spends more time computing more intermediate variables than the BCG-FFT method does. However, the most expensive computation for each of the two methods is the two linear operator computations mentioned before and the extra time for computing the intermediate variables is well compensated by its faster convergence rate. The maximum solution error for the internal electric field is 3.7%, 2.6%, 4.1% and 3.7% for CG-, BCG-, BCGS- and TFQMR-FFT methods, respectively. Note this error fluctuates from case to case for these methods, and does not indicate one method is more accurate than the other.

Figure 4 (a) and (b) give the log-log plots of the memory cost and the CPU time per iteration with respect to the number of unknowns for the above model, respec-

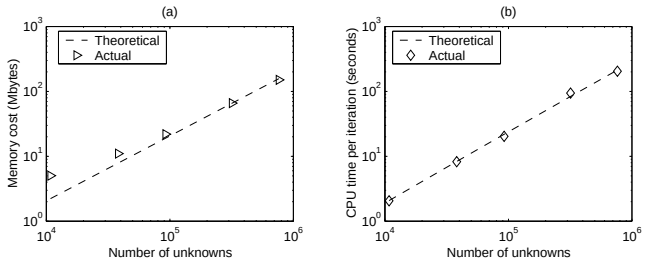

Fig. 4. The computer memory (a) and CPU time per iteration (b) versus the number of unknowns for the case in Figure 3.

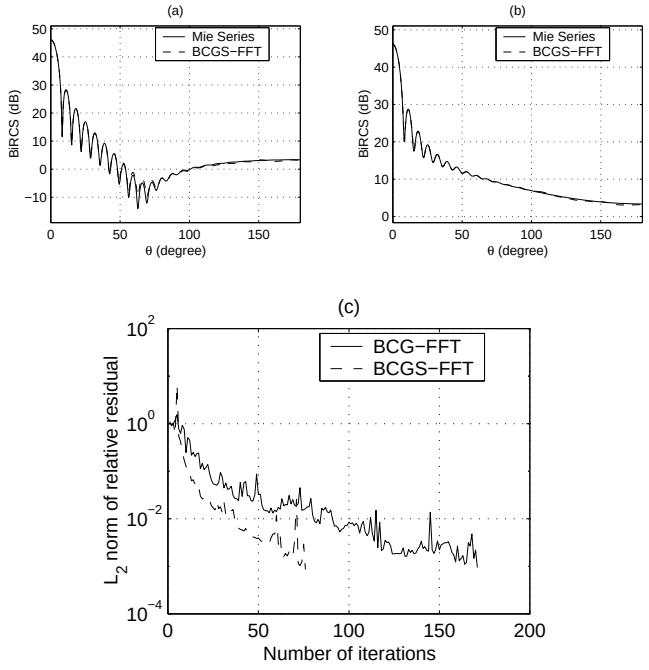

Fig. 5. The Bi-RCS of a two-layer sphere with $a_1 = 1.5075$ m, $\epsilon_{r,1} = 4.0$, $a_2 = 1.2075$ m, $\sigma_1 = 0.1$ S/m, $\epsilon_{r,2} = 2.0$ and $\sigma_2 = 0.05$ S/m from the BCGS-FFT method. (a) $\phi = 0$, (b) $\phi = \frac{\pi}{2}$, (c) the convergence curves.

tively. These plots confirm that the memory and CPU requirements of the BCGS-FFT method are $O(N_t)$ and $O(N_t \log N_t)$, respectively. Note that the first point of the memory plot has a small N_t and is not included in the least-square fitting because of its extra overhead; as a result, this point has a large deviation from the fitted curve.

The third model is a much larger two-layer sphere with the same geometry as in Figure 1. The model parameters are $a_1 = 1.0575$ m, $\epsilon_{r,1} = 4.0$, $\sigma_1 = 0.1$ S/m, $a_2 = 1.2075$ m, $\epsilon_{r,2} = 2.56$ and $\sigma_2 = 0.05$ S/m. The frequency of the incident plane wave is 1 GHz. The dimension of this scattering object is $14.1\lambda_{min} \times 14.1\lambda_{min} \times 14.1\lambda_{min}$, where λ_{min} is the wavelength in layer 1, and the number of unknowns

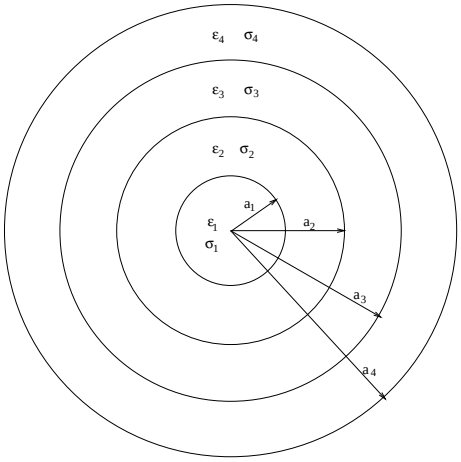

Fig. 6. The cross section of a four-layer concentric sphere with radius a_1, a_2, a_3, a_4, permittivity ϵ_1, ϵ_2, ϵ_3, ϵ_4 and conductivity σ_1, σ_2, σ_3, σ_4.

is $3 \times 162 \times 161 \times 161$=12,597,606, which gives a sampling rate of 11.5 points per minimum wavelength. Figure 5 (a) and (b) gives the bistatic RCS in $\phi = 0$ and $\phi = \pi/2$ of the BCGS-FFT method, respectively. The RMS errors of the RCS are 0.67 dB and 0.17 dB for these two curves. The convergence rates of the BCGS-FFT and BCG-FFT methods are shown in Figure 5 (c). The BCG-FFT converges after 171 iterations while the BCGS-FFT converges after 76 iterations. Again the BCGS-FFT method converges much faster than the BCG-FFT method. The total run time for the BCGS-FFT method is 26.17 CPU hours while that for the BCG-FFT method is 57.77 CPU hours. The memory cost is approximately 367 MB.

Figure 6 shows the cross section of a four-layer concentric sphere and Figure 7 (a) and (b) give the bistatic RCS of the model with radii of $a_1 = 0.1$ m, $a_2 = 0.2$ m, $a_3 = 0.3$ m, $a_4 = 0.48$ m, dielectric constants of $\epsilon_{r,1} = 4.0$, $\epsilon_{r,2} = 2.56$, $\epsilon_{r,3} = 2.25$, $\epsilon_{r,4}$=1.5, and conductivity of $\sigma_1 = 0.2$ S/m, $\sigma_2 = 0.08$ S/m, $\sigma_3 = 0.05$ S/m and $\sigma_4 = 0.01$ S/m. The RMS errors for these two curves are 0.53 dB and 0.39 dB, respectively. The frequency of the incident plane wave is 1 GHz and the number of unknowns is $3 \times 64 \times 63 \times 63$ =762,048. The memory cost is 77 MB. The total run time is 24.65 CPU minutes and the number of iterations is 17 for a residual of 0.1%. The convergence curve is shown in Figure 7(c). Thus the number of sampling points per minimum wavelength is 10. Note that the numerical result from the BCGS-FFT method and the analytical solution have a good agreement. Furthermore, the volume integral equation formulation is in general more efficient for these kinds of complicated geometries than the surface integral equation formulation.

The last model is the scattering from a finite dielec-

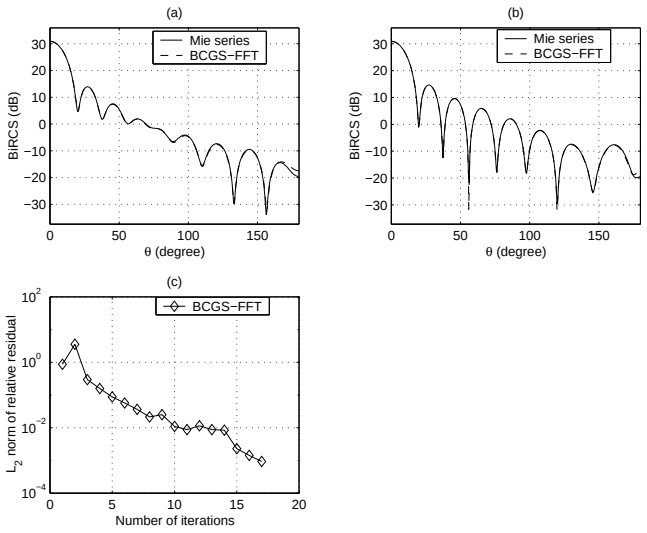

Fig. 7. The Bi-RCS of a four-layer concentric sphere in Figure 6 with radii $a_1 = 0.1$ m, $a_2 = 0.2$ m, $a_3 = 0.3$ m, $a_4 = 0.48$ m, dielectric constants $\epsilon_{r,1} = 4.0$, $\epsilon_{r,2} = 2.56$, $\epsilon_{r,3} = 2.25$, $\epsilon_{r,4} = 1.5$ and conductivity $\sigma_1 = 0.2$ S/m, $\sigma_2 = 0.08$ S/m, $\sigma_3 = 0.05$ S/m and $\sigma_4 = 0.01$ S/m. (a) $\phi = 0$, (b) $\phi = \frac{\pi}{2}$, (c) the convergence curve.

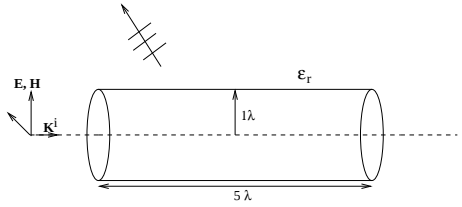

Fig. 8. The geometrical model for scattering from a finite dielectric cylinder.

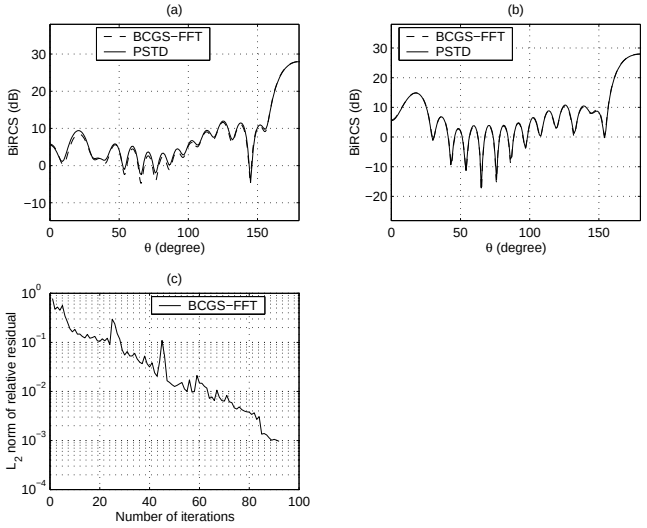

Fig. 9. The Bi-RCS results from the BCGS-FFT and PSTD methods [20] of the finite cylinder shown in Figure 8 with $\epsilon_r = 2.25$. (a) $\phi = 0$, (b) $\phi = \frac{\pi}{2}$, (c) the convergence curve.

tric cylinder. The dimension of the cylinder is shown in Figure 8, where λ is the wavelength of the incident field in free space and $\epsilon_r = 2.25$ is the dielectric constant of the cylinder. The number of unknowns is 1,146,231. The memory cost is about 70 MB and the total run time is 21.48 CPU hours. For an axial incident plane wave, the RCS of the cylinder from the BCGS-FFT method compared to that obtained from the pseudospectral time-domain (PSTD) method for the body of revolution (BOR) in [20] is given in Figure 9 (a) and (b). Note the excellent agreement between the two methods is within 1.5 decibels over a dynamic range of approximately 50 dB. The root mean square (RMS) error for $\phi = 0.0$ is 1.1212 dB and that for $\phi = 90.0$ is 0.7667 dB. Figure 9 (d) shows the convergence curve of the BCGS-FFT method for this model. As expected, the convergence rate is slower for this case because the cylinder is lossless.

IV. Conclusion

The main contribution of this work is the incorporation of the stabilized biconjugate-gradient method in an FFT accelerated volume integral equation solver. The BCGS-FFT method is applied to solve electromagnetic scattering from inhomogeneous penetrable objects. It converges much faster than the CG-FFT method and more smoothly and faster than BCG-FFT method. Typically, it requires a CPU time $1.5 - 2$ and $2.5 - 8$ times less than the BCG-FFT and CG-FFT methods, respectively. The BCGS-FFT method is an appealing choice for large scattering problems.

Acknowledgment

This work was supported by Environmental Protection Agency through a PECASE grant CR-825-225-010, and by the National Science Foundation through grants ECS-9702195 and CCR-00-98140. We thank Jan Hesthaven for providing the independent result in Figure 9 for validation. We also thank North Carolina Supercomputing Center for the use of a single processor from their SGI Origin 2400 cluster in some examples in this work.

References

[1] P. Zwamborn and P. M. van den Berg, "The three dimensional weak form of the conjugate gradient FFT method for solving scattering problems," *IEEE Trans. Microwave Theory and Tech.,* vol. 9, no. 40, pp. 1757-1766, 1992.

[2] H. Gan and W. C. Chew, "A discrete BCG-FFT algorithm for solving 3D inhomogeneous scatter problems," *J. Electromagn. Waves and Appl.,* vol. 9, no. 10, pp. 1339–1357, 1995.

[3] M. R. Hestenes and E. Stiefel, "Methods of conjugate gradients for solving linear systems," *J. Res. Nat. Bur. Stand.,* vol. 49, pp. 409–435, 1952.

[4] T. K. Sarkar, ed., *Application of conjugate gradient method to electromagnetics and signal analysis*, PIER 5, Progress in Electromagnetics Research, New York: Elsevier, 1991.

[5] T. K. Sarkar, "The application of conjugate gradient method the solution of operator equations arising in electromagnetic scattering from wire antennas," *Radio Science,* vol. 19, Sept.-Oct. 1984, pp. 1156-1172.
[6] T. K. Sarkar, "On the application of the generalized biconjugate gradient method," *J. Electromagn. Waves and Appl.,* vol. 1, no. 3, pp. 223–242, 1987.
[7] C. Lanczos, "An iteration method for the solution of the eigenvalue problem of linear differential and integral operators," *J. Res. Nat. Bur. Stand.,* vol. 45, pp. 255–282, 1950.
[8] C. Lanczos, "Solutions of systems of linear equations by minimized iterations," *J. Res. Nat. Bur. Stand.,* vol. 49, pp. 33-53, 1952.
[9] P. Sonneveld, CGS: "A fast Lanczos-type solver for nonsymmetric linear system," SIAM J. Sci. Statist. Comput., 10 (1989), pp. 36-52.
[10] H. A. van der Vorst, "Bi-CGSTAB: a fast and smoothly converging variant of Bi-CG for the solution of nonsymmetric linear systems," *SIAM J. Sci. Stat. Comput.,* vol. 13, no. 2, pp. 631-644, March 1992.
[11] T. F. Chan, E. Gallopoulos, V. Simoncini, T. Szeto and C. H. Tong, "A quasi-minimal residual variant of the BI-CGSTAB algorithm for nonsymmetric system," *SIAM J. Sci. Comput.,* vol. 15, no. 2, pp. 338-347, 1994.
[12] R. W. Freund, "A transpose-free quasi-minimal residual algorithm for non-Hermitian linear systems," *SIAM J. Sci. Comput.,* vol. 14, no. 2, pp. 470-482, March 1993.
[13] R. W. Freund and N. M. Nachtigal, "QMR, A quasi-minimal residual method for non-Hermitian linear systems," Numer. Math., 60 (1991), pp. 315-339.
[14] R. W. Freund and N. M. Nachtigal, "An implementation of the QMR method based on coupled two-term recurrences," SIAM J. Sci. Comput., 15 (1994), pp. 313-337.
[15] M. Sauren and H. M. Bucker, "On deriving the quasi-minimal residual method," SIAM Rev., vol. 40, no. 4, pp. 922-926, December 1998.
New York, Wiley, 1989.
[16] M. F. Catedra, R. P. Torres, J. Basterrechea, and E. Gago, *The CG-FFT Method: Application of Signal Processing Techniques to Electromagnetics*, Boston: Artech House, 1995.
[17] Z. Q. Zhang, and Q. H. Liu, "Three-dimensional weak-form conjugate- and biconjugate-gradient FFT methods for volume integral equations," *Microwave Opt. Tech. Lett.*, vol. 29, no. 5, pp. 350–356, 2001.
[18] C. F. Smith, A. F. Peterson, and R. Mittra, "The biconjugate gradient method for electromagnetic scattering," *IEEE Trans. Antenna Propagat.,* vol AP-38, no. 6, pp. 938–940, June 1990.
[19] W. C. Chew, *Waves and Fields in Inhomogeneous Media,* IEEE Press, 1995.
[20] B. Yang and J. S. Hesthaven, "A pseudospectral method for time-domain computation of electromagnetic scattering by bodies of revolution," *IEEE Trans. Antennas Propagat.*, vol. 47, pp. 132–141, 1999.